

Evaluation of the air quality in arid climate megacities (Case study: Greater Cairo)

Mohammed Mahmoud A. HWEHY^{1,2,*} , Fawzia Ibrahim MOURSY¹,
Attia Mahmoud EL-TANTAWI¹, Mostafa Abd El-Hameed MOHAMED¹

¹ Faculty of African Postgraduate Studies, Cairo University, Giza, Egypt

² Air Quality Department, Egyptian Environmental Affairs Agency, Cairo, Egypt

Abstract: The accelerated urbanization in the last decade and population growth in developing countries in the Middle East and North Africa (MENA) region have increased the count of humans exposed to air pollution. This work aims to provide an insight into air quality in the Greater Cairo (GC) area which is one of the largest megacities in the MENA region and is classified as its most polluted city according to the reports of the World Health Organization (WHO). Exploratory data analysis and cluster analysis were used to assess the pollutants data and meteorological data to understand the impacts of weather factors on air quality in GC. According to the results, GC suffers from particle matter of 10 micrometres or less (PM10) pollutants. The annual averages ranged from 97 ± 10 to $203 \pm 42 \mu\text{g}/\text{m}^3$. Though short-term exposure to gaseous pollutants did not exceed the limits, the long-term exposures exceeded those in some congested traffic areas. The annual averages ranged from 20 ± 5 to $63 \pm 24 \mu\text{g}/\text{m}^3$ for Nitrogen dioxide (NO_2) and from 9 ± 3 to $21 \pm 5 \mu\text{g}/\text{m}^3$ for sulphur dioxide (SO_2). Also, the terrain affects the spatial variation of pollutants observation. There is a negative correlation between the monitoring site elevation and the pollutant concentration.

Key words: air pollution, terrain, cluster analysis, particulate matter, nitrogen dioxide, sulphur dioxide

1. Introduction

Air pollution is defined as an imbalance in the chemical composition of the surrounding atmosphere, whether it is due to the difference in the proportions of its components or by the solid, liquid, or gaseous contaminants that are foreign to those components (*Harrop, 2002*). This imbalance causes changes in the atmospheric properties such as visibility and temperature and its mechanisms such as the hydrological cycle. In addition, it causes threats and dangers to human health, while air quality exceeds the WHO's

*corresponding author, e-mail: mohammed.hwehy@faps.cu.edu.eg

guideline in more than 90% of the places where people live around the world, deaths due to air pollutants are estimated to be around 4.2 million annually (Kuo et al., 2019).

Inhalable and respirable particulate matter with a diameter of 10 microns or less (PM₁₀), including fine particles less than 2.5 microns (PM_{2.5}) causes health risks, due to its capability of penetrating human lungs and entering the bloodstream (Xing et al., 2016). Nitrogen dioxide (NO₂) is an important product of secondary pollutants such as particulate matter and ozone. Moreover, it can increase symptoms of bronchitis and asthma, as well as cardiovascular and respiratory diseases (Peel et al., 2007). Sulphur dioxide (SO₂) affects the respiratory system and the function of the lungs and irritates the eyes. SO₂ combines with atmospheric water content to form acid rain (Katsouyanni, 2003).

Many studies assess the air quality in the MENA region (Abbass et al., 2018; Abera et al., 2021; Bauer et al., 2019; Petkova et al., 2013; Rees et al., 2019; Roy, 2016). In most of these previous studies, the WHO's guideline is used without regard to the effects of the geographical nature of the region, which necessitates that the criterion in assessing air quality is the interim targets issued by the WHO for countries that are encouraged to gradually achieve through enforcing stringent air quality control practices.

WHO uses the annual average of airborne particulate matter as an ambient air quality indicator. GC was recorded as one of the most polluted cities in the MENA region during the period from 2011 to 2015; PM₁₀ was greater than 150 µg/m³ (WHO, 2016).

The sources of air pollution in GC are known (Abbass et al., 2020; Aboel Fetouh et al., 2013; Favez et al., 2008; Heger et al., 2019; Hindy and Abdelmaksoud, 2016; Marey et al., 2010; Matysik et al., 2010; Mostafa et al., 2018, 2019; Wheida et al., 2018). It varies between the natural sources in the desert surrounding its southern regions and over a vast area extending across the Western Sahara and the Eastern Sahara. As well as anthropogenic sources, which vary between vehicle exhaust and open burning of waste, whether agricultural or municipal waste, in addition, to emissions of industrial facilities located at the planned and unplanned industrial areas, as they are spread throughout GC and their environmental loads vary.

There is no doubt that weather and topography affect the dispersion of air pollutants, either a negative effect or a positive effect. Land cover

and land use in GC vary greatly. While GC is surrounded by desert, the Nile Delta is in the northern part of it, while the middle area of GC is full of various anthropogenic activities and manifestations of urbanization, and this causes the phenomenon of heat islands inside the city (*Han et al., 2015; Kanakidou et al., 2011; Robaa, 2013*).

The current paper studied the correlation between the elevation of monitoring sites and pollutant concentration. Also, it updated the trend of long-term exposure to pollutants in GC. This paper assesses the recent compatibility of air quality in GC with the WHO’s guidelines. Also, it introduces an understanding of the effects of the weather, topography, and the daily anthropogenic routine on the air quality in GC.

2. Material and methods

2.1. Study area

Greater Cairo (GC) refers to Cairo Governorate (the Egyptian capital), in addition, to the populated areas in urban and semi-urban of Giza and Qalyubia governorates (*Salem et al., 2020*). Figure 1 shows that GC surrounds the banks of the Nile River, in the south of the Nile Delta agricultural areas, and is surrounded on the east, south, and west by the desert of the Cairo and Giza governorates. Also, it is a mixed area, due to some industrial areas side by side from residential areas, surrounded by a complex network of congested roads (*Ahmed et al., 2017*).

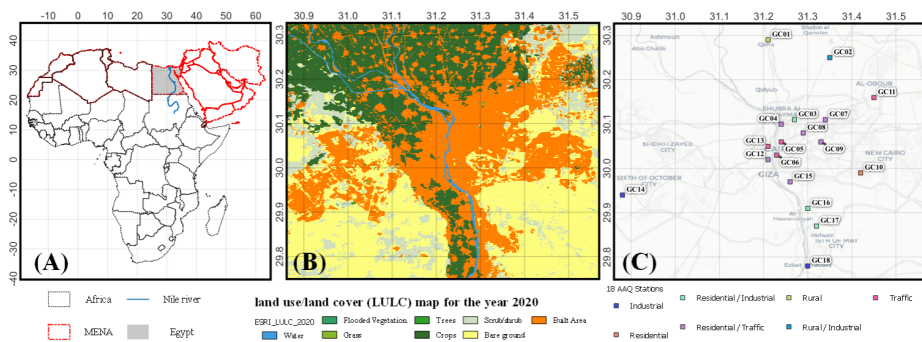


Fig. 1. Study area maps; (A) Africa (black dashes) and Middle East and North Africa MENA (red dashes) map, (B) Greater Cairo LULC, and (C) ambient air quality stations.

GC is dominated by a semi-tropical desert climate, which is characterized according to the Koeppen climate classification as hot and dry with a clear sky in summer, and moderate winters with little rain (*Beck et al., 2020; Zaki and Swelam, 2017*). This dry and desert climate causes desert nature to be one of the most important sources of total suspended particulate pollutants, whether they are triggered by sandstorms or by stimulating the movement of cars and pedestrians for the accumulated dust on the roads. This is a reason why particle averages exceed the levels stipulated by the WHO, and it becomes acceptable for these averages to be compared with the limits of the interim target (IT-1) (*WHO, 2000*) of the WHO to measure the extent of the ability to achieve and adhere to it.

2.2. Data

2.2.1. Air pollution data

The air pollutants data used are the hourly average data for PM₁₀, NO₂, and SO₂. They were obtained from the national network for ambient air quality monitoring that is owned and managed by the Egyptian Environmental Affairs Agency (EEAA) for the period beginning from January 1, 2010, through December 31, 2019.

Ambient air pollutant data from 18 continuous monitoring stations were used. The selected stations achieve operating rates of at least 18 hours daily and 75% of the year days during this period, according to the US EPA (*U.S. EPA, 2017*). Table 1 shows the location, elevations (metres above the mean sea level (MSL)), and classification of these stations. In addition to the 17 stations spread across the GC, the data of the Qaha station, which is outside the GC area, was taken as a close site in the north of the study area to represent the agriculture activities of the Nile Delta area.

2.2.2. Meteorological data

The effects of weather conditions on the air quality for the GC region were assessed by using the meteorological variables including wind speed (WS) and wind direction (WD), temperature (T), mean sea level (MSL) pressure, relative humidity (RH), horizontal visibility, and the Atmospheric Mixing Layer Height, in which the pollutants transfer, in addition to the recorded weather phenomena (sand (SA), sand storm (SS), dust (DU), haze (Hz), etc.).

Table 1. The stations' location, elevation, and classification.

Code	Station	Latitude (°)	Longitude (°)	Elevation (m)	Classification
GC01	Qaha	30.29	31.21	14	Rural
GC02	Abu Zabal	30.25	31.35	22	Rural / Industrial
GC03	Shobra	30.11	31.27	13	Residential / Industrial
GC04	El-Sahel	30.10	31.24	24	Residential / Traffic
GC05	Qullaly	30.06	31.24	27	Traffic
GC06	Qasr Aeny	30.03	31.23	27	Traffic
GC07	Heliopolis	30.11	31.34	48	Residential / Traffic
GC08	Abbasia	30.08	31.29	29	Residential / Traffic
GC09	Nasr City	30.06	31.33	94	Residential / Traffic
GC10	New Cairo	29.99	31.42	268	Residential
GC11	Sallam	30.16	31.45	67	Traffic
GC12	Giza Square	30.02	31.21	23	Residential / Traffic
GC13	Mohandisin	30.05	31.21	37	Traffic
GC14	6th October	29.94	30.88	137	Industrial
GC15	Maadi	29.97	31.26	29	Residential / Traffic
GC16	Massara	29.91	31.30	25	Residential / Industrial
GC17	Helwan	29.87	31.32	45	Residential / Industrial
GC18	Tibben	29.78	31.30	21	Industrial

The Weather observations data for Cairo airport station (WMO code: HECA) were obtained for a similar duration of the pollution data from the Iowa State University – Iowa Environmental Mesonota database of archives of automated airport weather observations Automated Surface Observing System ‘ASOS Metar’ and the Integrated Surface Dataset from NOAA National Center for Environmental Information NCEI (*Herzmann and Wolt, 2017; NOAA NCEI, 2001*).

For the ambient air monitoring stations without nearby weather stations, the Fifth-Generation Penn State/NCAR Mesoscale Model (MM5) was used to predict T, RH, WS, WD, and the height of the planetary boundary layer HPBL, which is an indicator of the atmospheric mixing layer height. The surface-level observations of Cairo Airport station and the Radiosonde observations of Helwan station, from the Integrated Global Radiosonde Archive IGRA (*Durre et al., 2006*), were used to evaluate the downscaled 12 km resolution output of the widely used fifth-generation mesoscale model

(MM5) developed by the National Center for Atmospheric Research in Pennsylvania State University (*Grell et al., 1994*).

Most monitoring stations were located at the same height from the ground level, about 10 meters approximately, so the elevation of the monitoring site was evaluated. The shuttle radar topography mission (SRTM) elevation data at a resolution of 30 metres was used. SRTM elevation data were obtained from the United States Geological Survey (USGS)'s Center of Earth Resources Observation and Science (EROS) (*USGS, 2018*). Global Land use and land cover (LULC) (*Karra et al., 2021*) was used in the study area map.

2.3. Methodology

Statistical analysis was used to explore the data, as measures of central tendency and measures of dispersion were calculated for the raw data obtained from the Environmental Affairs Agency, which represent hourly averages of pollutants at the selected stations, as the daily averages that were calculated after sparing the observations that were less than 75% of the hours of the day. Also, to describe meteorological variables, weather phenomena, and pollutants, the frequency was calculated.

The combined arithmetic average (Eq. (1)) (*Upton and Cook, 1996*) was used to calculate the weighted mean of separated data sets of pollutants in the study area for hours, days, and months to understand the temporal variation of the influence of human activity and the behaviour of atmospheric temperatures in the study area on the pollutants pattern. To clarify the pattern of different pollutants in the various analysed referred, range scaling of results using the minimum and maximum method was used.

$$\text{Combined arithmetic average: } \overline{X}_j = \frac{\sum_{i=1}^s n_{i,j} \overline{x}_{i,j}}{\sum_{i=1}^s n_{i,j}}, \quad (1)$$

where \overline{X}_j is the combined mean, $\overline{x}_{i,j}$ is the mean of the i -th station sample for a j -th pollutant, $n_{i,j}$ is the sample size of the i -th station sample for a j -th pollutant, and s is the total count of stations ($s = 18$).

Simple linear regression was used to detect the basic trend for each pollutant at each station. Hierarchical Cluster Analysis and K-means Cluster

Analysis (Adams, 2002) were employed as part of the tool kit for exploratory data analysis. Those cluster analysis methods are used as unsupervised multivariate analysis to identify groups of similar characteristics. Euclidean distance metric was used to describe dissimilarity and measure the distance between multidimensional data. For (m) variables, the Euclidean distance was given by the multidimensional Pythagorean equation (Eq. (2)) for all pairs of objects defined by the standardized variables:

$$\text{Euclidean distance: } d = \sqrt{\sum_{j=1}^m (xs_{i,j} - xs_{i',j})^2}, \quad (2)$$

$$\text{Standardized value: } xs_{i,j} = \frac{x_{i,j} - \bar{x}_{i,j}}{sd_{i,j}}, \quad (3)$$

where $xs_{i,j}$ is standardized value of of the i -th station sample for a j -th pollutant calculated in Eq. (3), and sd is the standard deviation.

Pearson correlation coefficient ($r\%$) and the range Normalized Root Mean Square Error (NRMSE) (Eq. (4)) were used to evaluate the MM5 output. The predicted values (P) from the MM5 compared against the observation (O) of Cairo airport station for surface-level and the Atmospheric Mixing Layer Height obtained from the radiosonde observation of Helwan station as determined using the parcel method (Li et al., 2021). The most important results of these analyses will also be discussed later. Also, the frequencies observed, and predicted wind speed and wind direction were compared.

$$\text{NRMSE } \% = \frac{\sqrt{\frac{(P - O)^2}{n_{P-O}}}}{\max(O) - \min(O)} * 100. \quad (4)$$

3. Results and discussion

3.1. Evaluation of MM5 output

Table 2 shows the results of the MM5 evaluation for surface T, RH, at 2 m above ground level (AGL), MSL pressure, and HPBL. Person correlation coefficient $r\%$ for hourly T and HPBL nare 76 and 68, respectively. For daily means of pressure and RH are 36 and 50, respectively. The low correlation for hourly and daily periods can be attributed to factors such as temporal

Table 2. statistical analysis of the MM5 model’s meteorological variable against the Cairo Airport meteorological station from January 2010 to December 2019.

Meteorological variable	Period	Calculation	r (%)	NRMSE (%)
Temperature (°C)	Hour	Record	76.41	22.2
	Daily	Mean	91.26	11.4
	Month	Mean	99.12	15.7
MSL Pressure (hPa)	Hour	Record	15.10	8.5
	Daily	Mean	36.64	7.7
	Month	Mean	99.65	4.9
Relative Humidity (%)	Hour	Record	40.89	8.5
	Daily	Mean	50.01	22.4
	Month	Mean	81.31	5.8
HPBL (m)	Hour	12 UTC	68.14	18.8
	Month	Mean	88.29	40.1
	Year	Mean	82.18	28.4

variability, model limitations, data quality issues, environmental influences, and the occurrence of extreme weather events. That indicates the MM5 model can predict temperature, and HPBL and less can predict pressure and RH%.

Table 3 shows the comparison between the observation and MM5 predicts wind components at 10 m (AGL). Mean wind speed is 3.9 and 3.8 (m/s) for observation and model, respectively. For observation and model, the Northern wind was 29.35 and 23.66%, respectively. Also, the light and mild winds were 62.84 and 67.52%, respectively. The near results made the model able to be used.

3.2. Summary of meteorological data

Meteorological data of the Cairo Airport observation station and the outputs of the MM5, for four sites representing the four main directions (North, East, South, and West), showed that the northern winds prevail over the study area with ratios of $25.5 \pm 3.0\%$, $14.3 \pm 3.6\%$, and $18.0 \pm 4.3\%$ for the north, northeast, and northwest winds, respectively. And it was $12.5 \pm 1.4\%$ and $6.4 \pm 0.5\%$ for the western and eastern winds, respectively.

Figure 2 shows the relative frequency distribution of wind categories. During the day, calm to light winds prevail during the early morning hours, creating haze conditions. During sunshine hours, mild and moderate winds

Table 3. Comparing the modelled data (M) for wind direction (a) and wind classes (b) from January 2010 to December 2019 with the observation at Cairo Airport station (O).

(a)

Wind Directions (°)	Observation (%)	Model (%)	O – M	
N	337.5 – 22.5	29.35	23.66	5.69
NE	22.5 – 67.5	19.31	11.87	7.44
E	67.5 – 112.5	6.90	6.42	0.48
SE	112.5 – 157.5	1.67	3.28	–1.61
S	157.5 – 202.5	5.58	3.43	2.15
SW	202.5 – 247.5	5.56	7.51	–1.95
W	247.5 – 292.5	8.43	13.86	–5.43
NW	292.5 – 337.5	15.37	21.54	–6.16

(b)

Wind Classes (m/s)	Observation (%)	Model (%)	O – M	
Calms	≤ 1	6.48	8.41	–1.92
light	1.00 – 3.00	24.24	25.86	–1.61
Mild	3.00 – 5.00	38.60	41.66	–3.06
Moderate	5.00 – 7.00	21.71	16.92	4.78
Active	7.00 – 9.00	5.96	4.37	1.59
Gust	≥ 9.00	1.66	2.76	–1.09
Missing	–	1.32	0	1.32
Mean	(m/s)	3.90	3.81	0.09

prevail. Active winds and storms often appear with the advancement of daylight hours. It was also found that the highest frequency of calm winds is from November to February, and the lowest is during the summer months.

Active and stormy winds are highest during the winter and spring months, and the lowest is otherwise. A wind rose in Figure 3 studied the winds associated with the recorded observations of dust and sand, it shows that the prevailing winds at the time of dust storms are Southwest, South, and West, respectively, and the frequencies of wind higher than 5 m/s exceed 86%.

The daily pattern of haze showed a weak negative correlation (-0.29) with temperature, on the contrary, it was a strong positive correlation (0.82) between temperature and the frequency of dust and sand events. Figure 4 shows the frequency of haze during the day. Haze has a higher frequency during the night than during the daytime. Also, the highest values are at

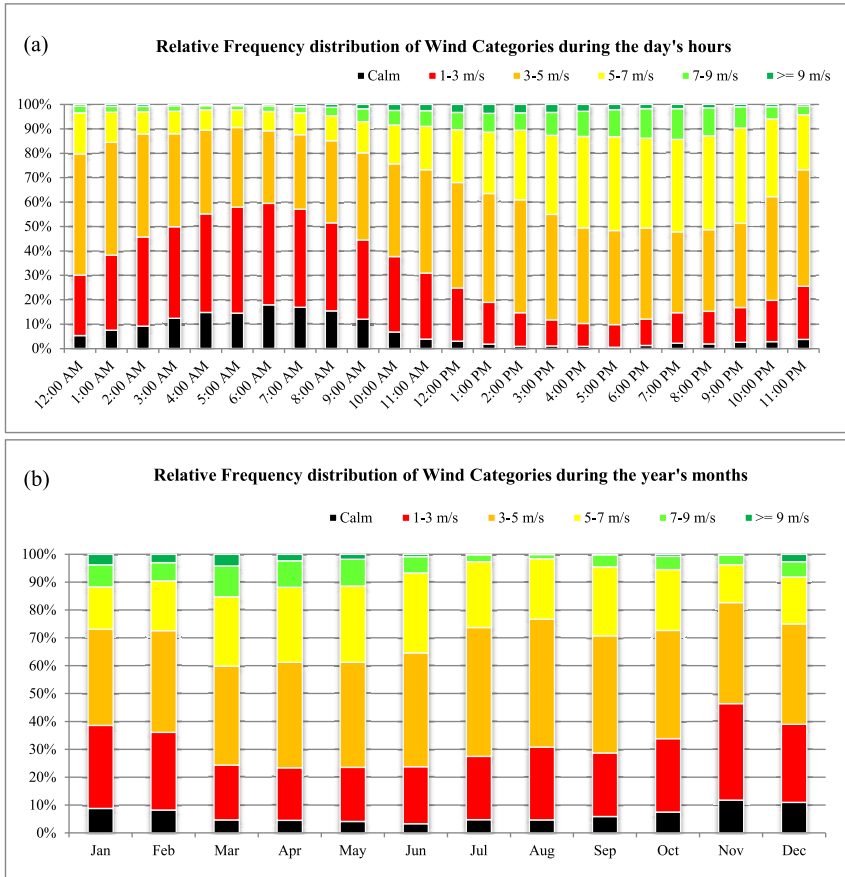


Fig. 2. Relative frequency distribution of wind categories during 2010–2019 observation at Cairo Airport station for (a) daily hours and (b) months.

the onset of human activity in the morning, but it decreases with the temperature increases. As for the events of dust and sand, their frequency often increases with the progression of the daylight hours.

Human activities are the source of the haze that appears in the atmosphere and affects visibility before it is cleared by natural factors (Yang et al., 2016). Figure 5 shows the hourly frequency of haze during the weekdays. It illustrates that vehicle exhausts have the greatest effect, as higher values show it with traffic density hours in GC (Ali and Tamura, 2002),

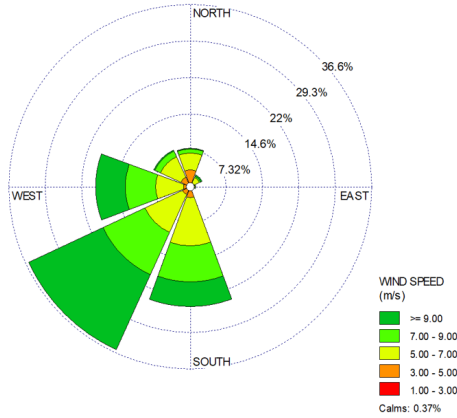


Fig. 3. Wind Rose during dust and sand hours for the period 2010–2019 observation at Cairo Airport station.

which are related to working hours. It also shows the lowest frequencies on Friday, which is the weekend. And there appears a pattern extended during Thursday afternoon, which may explain as high traffic due to most the non-indigenous residents traveling to neighboring cities to spend their weekends, in contrast to an extended pattern during Saturday, which is the day of the return of travellers.

3.3. Description of ambient air monitoring data

Exploratory data analysis (EDA) was applied to the hourly data obtained from EEAA and to the calculated daily average. Table 4 lists the WHO air quality guideline (interim target 1 for PM₁₀) and the regulatory standards of the Egyptian Law of Environment (EEAA's executive regulation) (*EL 4/1994* – Egyptian Law for the Protection of the Environment Number 4/1994 amended by Law Number 9/2009 and its Executive Regulation, 2009) The box plot, which is one of the EDA techniques used for data summarization and shown in Fig. 6, shows those guidelines of WHO and EEAA were achieved for both NO₂ and SO₂ whether for the hourly and the daily averages as short-term exposure to gases pollutants. Additionally, the daily averages appeared as hourly averages due to the minimal daily variations of SO₂. Oppositely for the daily averages of the PM₁₀, the results showed that the standards were exceeded in varying proportions between

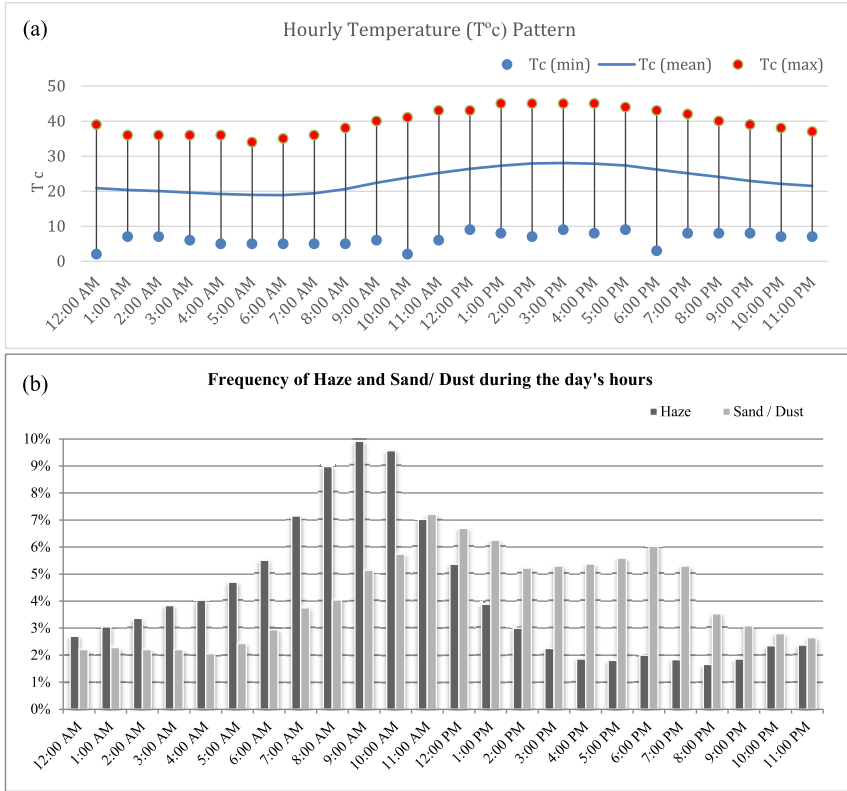


Fig. 4. (a) displays the hourly temperature data summary (line represents average, extreme events are represented by min blue pollute and max red pollute); and (b) relative frequency distribution of haze and dust/ Sand events during 2010–2019 observation at Cairo Airport station.

the studying stations, where the GC2, GC5, and GC16 stations have a higher median than $150 \mu\text{g}/\text{m}^3$, on the other hand, the third quartile for the stations GC8, GC9, GC10 and, GC12 are less than $150 \mu\text{g}/\text{m}^3$. That highly agrees with the results of *Wheida et al. (2018)* in their study of pollutants in GC for the duration beginning from 2010 to 2015.

3.3.1. Spatial variation of daily averages of pollutants

The first finding indicates that there is an inverse link between the mean of these data and the elevation of the station (-0.62 , -0.25 , and -0.16 for

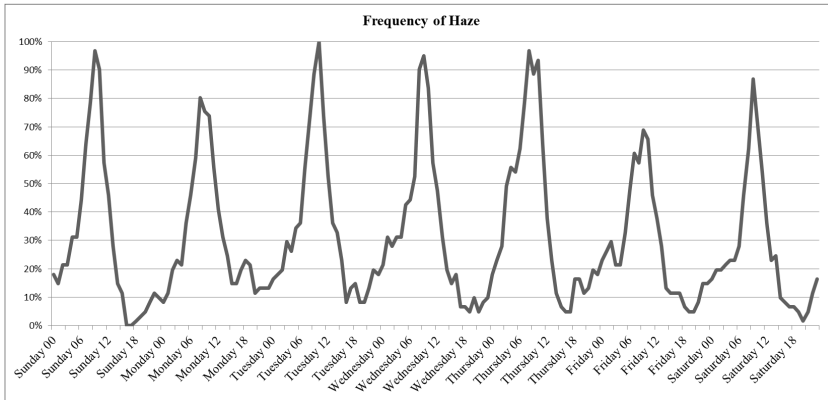


Fig. 5. Relative Frequency distribution per weekdays and hours of Haze during 2010 – 2019 observation at Cairo Airport station.

Table 4. The WHO air quality guideline (interim target 1 for PM10) and the Egyptian Law of Environment’s regulatory standards (EEAA’s executive regulation).

Pollutant, unit	Period	Area classification	WHO, IT 1	EEAA
PM10 ($\mu\text{g}/\text{m}^3$)	Daily	–	150	150
	Annual	–	70	70
SO ₂ ($\mu\text{g}/\text{m}^3$)	Hourly	Urban	500	300
		Industrial		350
	Daily	Urban	125	125
		Industrial		150
	Annual	Urban	20	50
		Industrial		60
NO ₂ ($\mu\text{g}/\text{m}^3$)	Hourly	–	200	300
	Daily	–	–	150
	Annual	Urban	40	60
		Industrial		80

PM10, SO₂, and NO₂, respectively) when looking at the daily average data for stations that represent a short-term exposure. Figure 7 shows that most of the stations, which have the smallest height MSL, located in the Basin of the Nile River exceeded the PM10’s daily standard of more than 25% of the actual operation days during the study period. The largest results were for stations GC02, GC16, and GC05 where the annual averages standard devi-

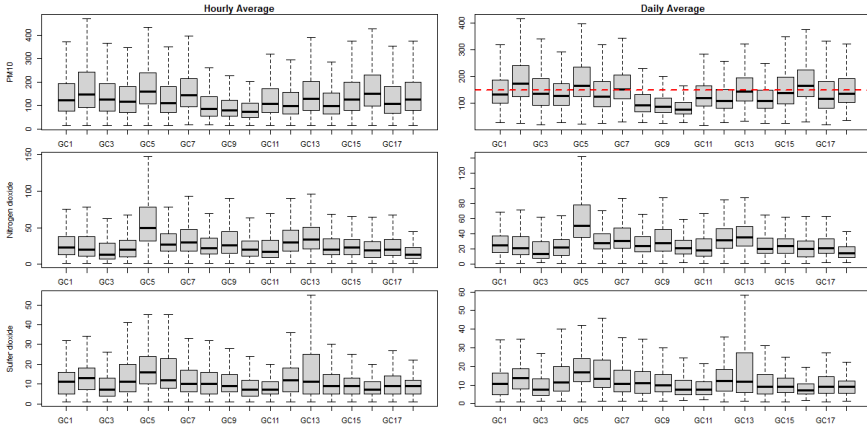


Fig. 6. Box plot showing PM10, NO₂, and SO₂ ($\mu\text{g}/\text{m}^3$) hourly and daily averages from January 2010 to December 2019.

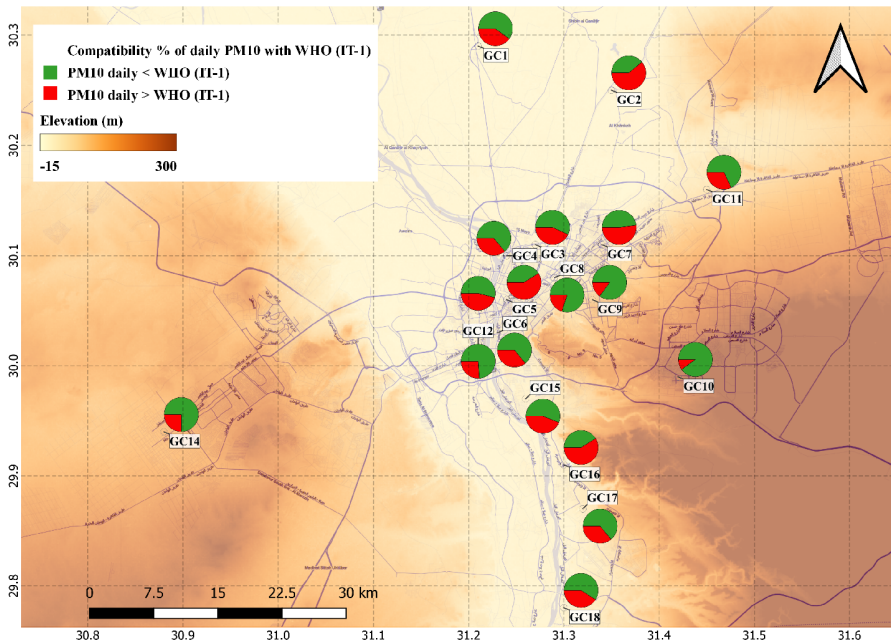


Fig. 7. The percentage of daily averages of PM10 for ambient air quality stations in Greater Cairo from January 2010 to December 2019, which is in line with Egyptian environmental laws and WHO recommendations.

ation were 203 ± 42 , 196 ± 40 , and 193 ± 31 , respectively. Otherwise, station GC10, which is located at the Mokattam hill and has the highest elevation, had the least average (Mean = 97, SD = 85). The inverse relationship between the station's elevation and pollutants concentration confirms that pollution is affected by topographic characteristics (*Mostafa et al., 2018*).

Table 5 shows the annual averages studied as long-term exposure, the PM10 exceeded WHO's guidelines and EEAA's standards. Though both SO₂ and NO₂ did not exceed the WHO's guideline or EEAA's standard for short-term exposure, the high-traffic areas located at mid of the Nile basin exceeded the long-term exposure standards. The annual average of NO₂ exceeded the WHO's guideline in almost all traffic and industrial areas, especially the centre of the city which exceeded EEAA's standards. This was less stressful for SO₂, as it exceeded the WHO's guideline in some stations,

Table 5. Averages of Annual means of pollutants, standard deviation, and slop of simple linear regression of each pollutant and time (10 years).

Station	PM10 ($\mu\text{g}/\text{m}^3$)			NO ₂ ($\mu\text{g}/\text{m}^3$)			SO ₂ ($\mu\text{g}/\text{m}^3$)		
	Mean	SD	Slope	Mean	SD	Slope	Mean	SD	Slope
GC01	161	41	-12	30	13	0	13	6	1
GC02	203	42	-10	25	11	2	14	5	1
GC03	163	49	-9	25	16	2	11	4	-1
GC04	148	33	-6	25	8	0	15	6	1
GC05	193	40	-6	63	24	6	21	5	1
GC06	152	37	-8	36	11	-1	18	8	1
GC07	178	25	5	33	14	0	14	6	1
GC08	116	23	-3	30	10	1	14	7	0
GC09	105	18	-3	34	10	2	12	4	1
GC10	97	10	-1	25	7	1	11	4	0
GC11	149	18	3	24	10	3	9	3	1
GC12	129	27	-6	37	12	2	14	6	1
GC13	165	31	-9	38	13	3	18	11	3
GC14	134	31	-5	27	9	2	12	6	1
GC15	163	46	-10	26	9	0	11	4	0
GC16	196	31	-4	24	10	2	10	3	1
GC17	149	32	-5	32	14	0	12	4	0
GC18	166	14	0	20	5	0	10	3	1

especially those located in traffic areas due to the low sulphur content in gasoline fuel used in vehicles. The basic trends of pollutants detected for each station showed that negative trend of PM10 annual means for most of the stations except for high-traffic stations GC07 and GC11 shown a positive trend. Also, industrial and traffic stations showed a positive trend for gas pollutants. The negative trend of GC01 station, which indicates the agricultural activities, proves the success of the efforts of Egyptians to prevent uncontrolled biomass burning.

The hierarchical cluster analysis, whether average or complete methods for calculating dissimilarity, used to explore the spatial variability of ambient air pollutant monitoring data indicated that the air quality in GC can be classified into three main clusters as shown in dendrogram in Fig. 8. The first cluster includes GC10 and GC14, both were the lowest in the pollu-

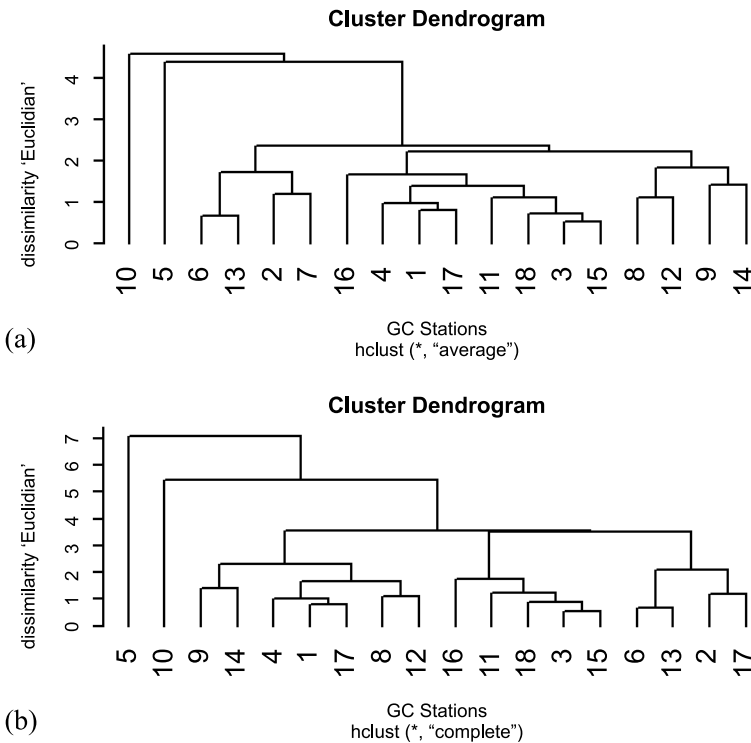


Fig. 8. Dendrogram tree represents the ambient air quality stations' clusters (a) average and (b) complete methods during 2010–2019.

tant’s concentration, respectively. Although the two stations are in different areas (GC10 residential areas and GC14 industrial areas), this cluster represents the effect of elevation. The second cluster consists of GC05, which was the highest pollutants exceeding standards. The third cluster includes the rest of the stations located between the two previous classifications. This indicated that traffic areas are the highest in the concentration of pollutants, then industrial areas, mixed areas, and finally residential areas. The concentration of pollutants gradually decreases with elevation (MSL) increasing.

The K-Mean cluster analysis, which is assigned to the classes containing its nearest neighbour based on similarity measured by distance, also agreed

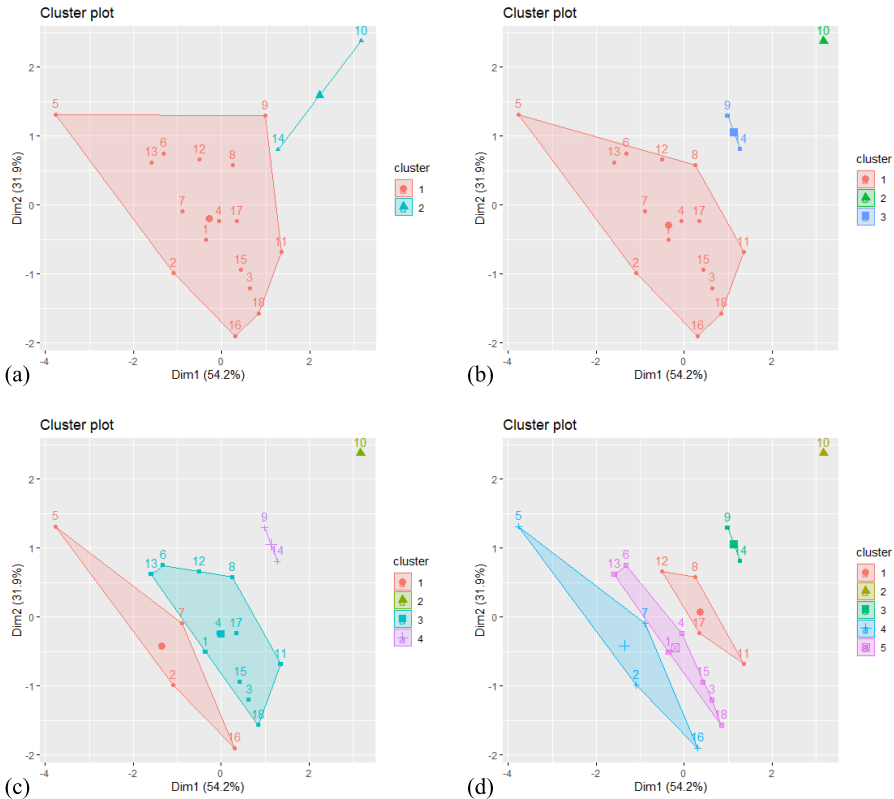


Fig. 9. DK-Mean cluster analysis for GC station, $k = 2, 3, 4,$ and 5 for (a), (b), (c), and (d), respectively.

with this result and the classification was done by placing a value of K equal to (2, 3, 4, and 5). Figure 9 shows the station must be grouped into more than two groups and the best result where $k = 3$ or 4. Also, GC10 has a unique behaviour. However, CG14 is classified as an industrial area, it is like GC09, which is a residential/ traffic area, due to the highest elevation of GC14. Oppositely, GC05 is a sign for the stations of the highly polluted areas. Generally, undesigned industrial areas (GC02, GC03, and GC16), high traffic with low elevation areas (GC05, GC06, GC11, GC12, and GC13), and controlled industrial areas (GC17 and GC18) have the efforts on air pollution in GC, respectively.

3.3.2. Temporal variation of pollutants data

Figure 10 shows the combined arithmetic averages, which are calculated for the hourly and daily averages. It showed that the variation in the levels of pollutants during the hours or the days was related to human activities. Pollutants begin to increase with the onset of human activity and are at their lowest levels during the hours of the night or the rest of the residents of GC. PM10 and NO₂ have two peaks during the day, which meet the two peaks of traffics density (Ali and Tamura, 2002; Heger et al., 2019). It is also clear that the lowest level of all pollutants was Friday, which is the weekly holiday in Egypt. The most important observation was the refraction of pollutant levels with the increase in the maximum temperatures during the day, which indicates the effect of increasing the mixing layer height below the planetary boundary layer as well as the increase in wind speeds on the dispersion of pollutants in GC. The variation in the level of the combined arithmetic averages for the months during the year confirmed that the level of pollutants is at its lowest levels during the summer months, which indicates the effect of increasing the planetary boundary layer height and increasing the average temperatures, which has an impact on the improvement of air quality in GC.

4. Conclusion

Exploratory data analysis (EDA) of pollutants in GC clearly showed that the issue of air pollution is due to the problem of increasing particulate

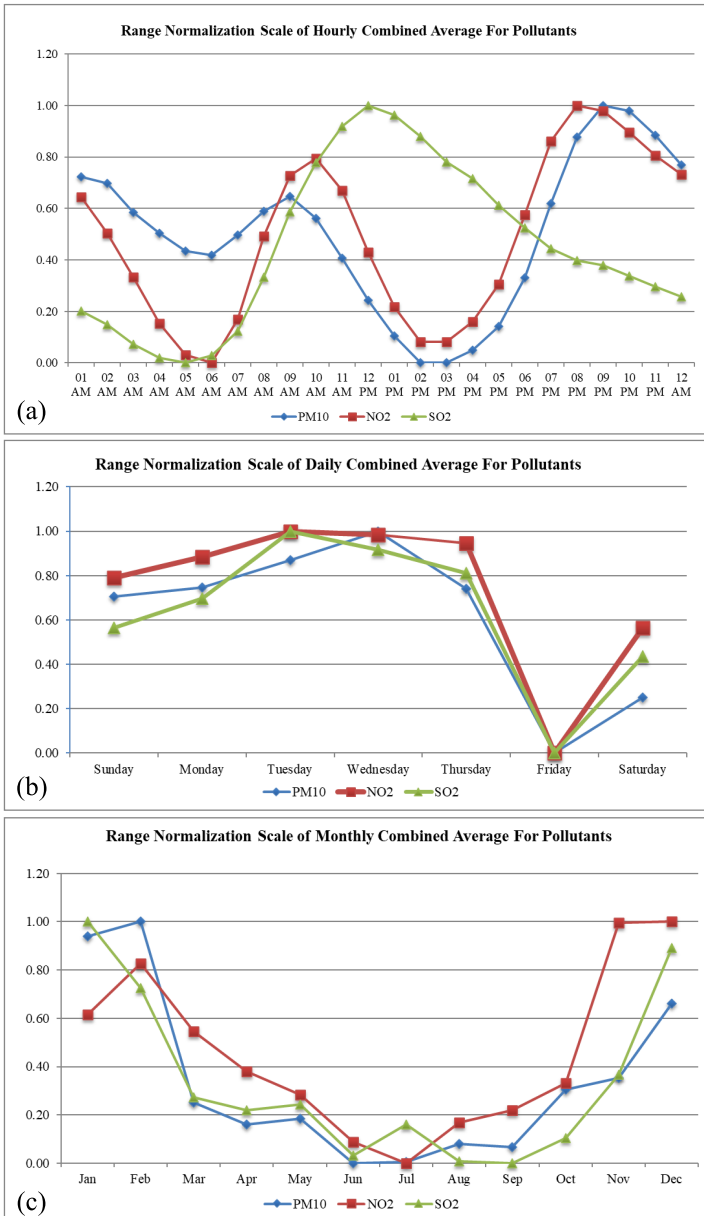


Fig. 10. Variation pattern of the pollutants (a) hourly, (b) weekdays, and (c) months for the ambient air quality stations during 2010–2019.

matter concentrations, whether in short-term exposure or long-term exposure. As for gaseous pollutants, they did not exceed the guidelines of WHO or the regulations of the Egyptian Environmental Law for short-term exposure, and some violations were recorded in areas with high traffic or heavy industrial activity for long-term exposure.

It turns out that sandstorms in GC are associated with gusty southern winds higher than 5 m/s. Its frequency is significantly higher with advancement in the hours of the day than during the night. On the contrary, the haze occurs during calm winds of less than 3 m/s, and their highest frequency is during the early morning hours, and gradually fades with progress in the daylight hours. In general, during daylight hours, weather factors help to disperse local pollutants due to the moderate winds and increasing mixing layer height. While the weather factors help the concentration of pollutants during the early morning and evening hours, due to the calm winds and the decreasing mixing layer height.

As for the annual pattern, the weather factors help to disperse local pollutants during the summer months due to wind speeds are higher than in the winter months, and the mean mixing layer height increases due to the mean temperature increases. The effect of the terrain is also evident on the dispersal of local pollutants, as there was a positive correlation between the elevation of the monitoring sites and pollutant averages. This caused stations located at the Nile River basin to have higher concentrations.

This suggests that the sources of pollution in GC are either natural sources as a result of raising the accumulated dust with the wind blowing or as a result of traffic congestion and large, planned, or small and craft industrial activities. Recent results indicate the successful control of the open burning of agricultural residues and biomass due to the efforts of the Egyptian Ministry of Environment in confronting episodes of acute air pollution.

Acknowledgements. The authors express their sincere gratitude to the Egyptian Environmental Affairs Agency (EEAA) for providing the data essential for this research.

References

Abbass R. A., Kumar P., El-Gendy A., 2018: An overview of monitoring and reduction strategies for health and climate change related emissions in the Middle East and

- North Africa region. *Atmos. Environ.*, **175**, 33–43, doi: 10.1016/j.atmosenv.2017.11.061.
- Abbass R. A., Kumar P., El-Gendy A., 2020: Car users exposure to particulate matter and gaseous air pollutants in megacity Cairo. *Sustain. Cities Soc.*, **56**, 102090, doi: 10.1016/j.scs.2020.102090.
- Abera A., Friberg J., Isaxon C., Jerrett M., Malmqvist E., Sjöström C., Taj T., Vargas A. M., 2021: Air quality in Africa: Public health implications. *Annu. Rev. Public Health*, **42**, 193–210, doi: 10.1146/annurev-publhealth-100119-113802.
- Aboul Fetouh Y., El Askary H., El Raey M., Allali M., Sprigg W. A., Kafatos M., 2013: Annual patterns of atmospheric pollutions and episodes over Cairo Egypt. *Adv. Meteorol.*, **2013**, 1–11, doi: 10.1155/2013/984853.
- Adams M. J., 2002: Chemometric tools and techniques in environmental monitoring. In: Burden F. R., McKelvie I., Forstner U., Guenther A. (Eds.): *Environmental monitoring handbook*. McGraw-Hill New York.
- Ahmed S., Ibrahim R. F., Hefny H. A., 2017: GIS-based network analysis for the roads network of the Greater Cairo area. *CEUR Workshop Proceedings*, 2144.
- Ali S. A., Tamura A., 2002: Road traffic noise mitigation strategies in Greater Cairo, Egypt. *Appl. Acoust.*, **63**, 11, 1257–1265, doi: 10.1016/S0003-682X(02)00046-4.
- Bauer S. E., Im U., Mezuman K., Gao C. Y., 2019: Desert dust, industrialization, and agricultural fires: Health impacts of outdoor air pollution in Africa. *J. Geophys. Res. Atmos.*, **124**, 7, 4104–4120, doi: 10.1029/2018JD029336.
- Beck H. E., Zimmermann N. E., McVicar T. R., Vergopolan N., Berg A., Wood E. F., 2020: Publisher correction: Present and future Köppen–Geiger climate classification maps at 1-km resolution. *Sci. Data*, **7**, 1, 274, doi: 10.1038/s41597-020-00616-w.
- Durre I., Vose R. S., Wuertz D. B., 2006: Overview of the integrated global radiosonde archive. *J. Clim.*, **19**, 1, doi: 10.1175/JCLI3594.1.
- EL 4/1994: Egyptian law for the protection of the environment number 4/1994 amended by law number 9/2009 and its executive regulation (2009). <http://www.eeaa.gov.eg/en-us/laws/envlaw.aspx>.
- Favez O., Cachier H., Sciare J., Alfaro S. C., El-Araby T. M., Harhash M. A., Abdelwahab M. M., 2008: Seasonality of major aerosol species and their transformations in Cairo megacity. *Atmos. Environ.*, **42**, 7, 1503–1516, doi: 10.1016/j.atmosenv.2007.10.081.
- Grell G., Dudhia J., Stauffer D. R., 1994: A description of the fifth-generation Penn State/NCAR Mesoscale Model (MM5). In: NCAR technical note NCAR/TN-398+STR, **115**, December. Mesoscale and Microscale Meteorology Division, National Center for Atmospheric Research.
- Han L., Zhou W., Li W., Meshesha D. T., Li L., Zheng M., 2015: Meteorological and urban landscape factors on severe air pollution in Beijing. *J. Air Waste Manage. Assoc.*, **65**, 7, 782–787, doi: 10.1080/10962247.2015.1007220.
- Harrop D. O., 2002: *Air Quality Assessment and Management: A Practical Guide* (Clay's Library of Health and the Environment). CRC Press, ISBN 9780415234115, 400 p.

- Heger M., Wheeler D., Zens G., Meisner C., 2019: Motor vehicle density and air pollution in Greater Cairo: fuel subsidy removal and metro line extension & their effect congestion and pollution? World Bank, Washington, DC, doi: 10.1596/32512.
- Herzmann D., Wolt J., 2017: IEM representivity analysis. Iowa State University Iowa Environmental Mesonet. Accessed at <http://mesonet.agron.iastate.edu/info/nni.phtml>.
- Hindy K. T., Abdelmaksoud A. S., 2016: Air quality monitoring around the first ISCC power plant in Egypt. *Water Air Soil Pollut.*, **227**, 2, 59, doi: 10.1007/s11270-015-2743-5.
- Kanakidou M., Mihalopoulos N., Kindap T., Im U., Vrekoussis M., Gerasopoulos E., Dermitzaki E., Unal A., Koçak M., Markakis K., Melas D., Kouvarakis G., Youssef A. F., Richter A., Hatzianastassiou N., Hilboll A., Ebojie F., Wittrock F., von Savigny C., Burrows J. P., Moubasher H., 2011: Megacities as hot spots of air pollution in the East Mediterranean. *Atmos. Environ.*, **45**, 6, 1223–1235, doi: 10.1016/j.atmosenv.2010.11.048.
- Karra K., Kontgis C., Statman-Weil Z., Mazzariello J. C., Mathis M., Brumby S. P., 2021: Global land use/land cover with Sentinel 2 and deep learning. In: Proc. 2021 IEEE International Geoscience and Remote Sensing Symposium IGARSS, Brussels, Belgium, 11-16 July 2021, 4704–4707, doi: 10.1109/IGARSS47720.2021.9553499.
- Katsouyanni K., 2003: Ambient air pollution and health. *Br. Med. Bull.*, **68**, 1, 143–156, doi: 10.1093/bmb/1dg028.
- Kuo C.-Y., Chan C.-K., Wu C.-Y., Phan D.-V., Chan C.-L., 2019: The short-term effects of ambient air pollutants on childhood asthma hospitalization in Taiwan: A national study. *Int. J. Environ. Res. Public Health*, **16**, 2, 203, doi: 10.3390/ijerph16020203.
- Li H., Liu B., Ma X., Jin S., Ma Y., Zhao Y., Gong W., 2021: Evaluation of retrieval methods for planetary boundary layer height based on radiosonde data. *Atmos. Meas. Tech.*, **14**, 9, 5977–5986, doi: 10.5194/amt-14-5977-2021.
- Marey H. S., Gille J. C., El-Askary H. M., Shalaby E. A., El-Raey M. E., 2010: Study of the formation of the “black cloud” and its dynamics over Cairo, Egypt, using MODIS and MISR sensors. *J. Geophys. Res. Atmos.*, **115**, D21, D21206, doi: 10.1029/2010JD014384.
- Matysik S., Ramadan A. B., Schlink U., 2010: Spatial and temporal variation of outdoor and indoor exposure of volatile organic compounds in Greater Cairo. *Atmos. Pollut. Res.*, **1**, 2, 94–101, doi: 10.5094/APR.2010.012.
- Mostafa A. N., Zakey A. S., Monem S. A., Abdel Wahab M. M., 2018: Analysis of the surface air quality measurements in the Greater Cairo (Egypt) metropolitan. *Glob. J. Adv. Res.*, **5**, 6, 207–214.
- Mostafa A. N., Zakey A. S., Alfaro S. C., Wheida A. A., Monem S. A., Abdul Wahab M. M., 2019: Validation of RegCM-CHEM4 model by comparison with surface measurements in the Greater Cairo (Egypt) megacity. *Environ. Sci. Pollut. Res.*, **26**, 23, 23524–23541, doi: 10.1007/s11356-019-05370-0.
- NOAA NCEI, 2001: Global surface hourly integrated surface dataset. <https://www.ncei>

- [.noaa.gov/metadata/geoportal/rest/metadata/item/gov.noaa.ncdc%3AC00532/html#](https://www.noaa.gov/metadata/geoportal/rest/metadata/item/gov.noaa.ncdc%3AC00532/html#).
- Peel J. L., Metzger K. B., Klein M., Flanders W. D., Mulholland J. A., Tolbert P. E., 2007: Ambient air pollution and cardiovascular emergency department visits in potentially sensitive groups. *Am. J. Epidemiol.*, **165**, 6, 625–633, doi: 10.1093/aje/kwk051.
- Petkova E. P., Jack D. W., Volavka-Close N. H., Kinney P. L., 2013: Particulate matter pollution in African cities. *Air Qual. Atmos. Health*, **6**, 3, 603–614, doi: 10.1007/s11869-013-0199-6.
- Rees N., Wickham A., Choi Y., 2019: Silent suffocation in Africa: Air pollution is a growing menace, affecting the poorest children the most. World Health Organization, accessed at: https://www.unicef.org/media/55081/file/Silent_suffocation_in_africa_air_pollution_2019.pdf.
- Robaa S. M., 2013: Some aspects of the urban climates of Greater Cairo region, Egypt. *Int. J. Climatol.*, **33**, 15, 3206–3216, doi: 10.1002/joc.3661.
- Roy R., 2016: The cost of air pollution in Africa. OECD Development Centre Working Papers, No. 333, doi: 10.1787/18151949.
- Salem M., Tsurusaki N., Divigalpitiya P., 2020: Land use/land cover change detection and urban sprawl in the peri-urban area of greater Cairo since the Egyptian revolution of 2011. *J. Land Use Sci.*, **15**, 5, 592–606, doi: 10.1080/1747423X.2020.1765425.
- Upton G., Cook I., 1996: *Understanding Statistics*. OUP Oxford, 657 p.
- U.S. EPA, 2017: *Quality assurance handbook for air pollution measurement systems: Ambient air quality monitoring program (Volume II)*. U.S. Environmental Protection Agency, Office of Air Quality Planning and Standards, Air Quality Assessment Division, RTP: Research Triangle Park, NC, USA, EPA-454/B-17-001.
- USGS, 2018: USGS EROS archive – Digital elevation – Shuttle radar topography mission (SRTM) 1 Arc-Second Global. Earth Resources Observation and Science (EROS) Center, doi: 10.5066/F7PR7TFT.
- Wheida A., Nasser A., El Nazer M., Borbon A., Abo El Ata G. A., Abdel Wahab M., Alfaro, S. C., 2018: Tackling the mortality from long-term exposure to outdoor air pollution in megacities: Lessons from the Greater Cairo case study. *Environ. Res.*, **160**, 223–231, doi: 10.1016/j.envres.2017.09.028.
- WHO, 2016: *Ambient air pollution: a global assessment of exposure and burden of disease*. *Clean Air J.*, **26**, 2, World Health Organization, doi: 10.17159/2410-972x/2016/v26n2a4.
- WHO, 2000: *Air Quality Guidelines for Europe, 2nd Ed.* WHO Regional Publications, European Series, No. 91, 1–185.
- Xing Y.-F., Xu Y.-H., Shi M.-H., Lian Y.-X., 2016: The impact of PM2.5 on the human respiratory system. *J. Thorac. Dis.*, **8**, 1, E69–E74, doi: 10.3978/j.issn.2072-1439.2016.01.19.
- Yang X., Zhang Z., Zhang Z., Sun L., Xu C., Yu L., 2016: A long-term prediction model of Beijing haze episodes using time series analysis. *Comput. Intell. Neurosci.*, **2016**, 6459873, doi: 10.1155/2016/6459873.

Zaki A., Swelam A., 2017: The Climatology of Nile Delta, Egypt. Amman, Jordan: International Center for Agricultural Research in the Dry Areas (ICARDA), <https://repo.mel.cgiar.org/handle/20.500.11766/6384>.